GEOSTATISTICAL ANALYSIS AND MITIGATION OF ATMOSPHERIC PHASE SCREENS IN KU-BAND TERRESTRIAL RADAR INTERFEROMETRY

Simone Baffelli[1] *Othmar Frey*[1,2] *Irena Hajnsek*[1,3]

(1) Chair of Earth Observation and Remote Sensing, ETH Zurich, Switzerland
(2)Gamma Remote Sensing AG, Gümligen, Switzerland
(3)Microwaves and Radar Institute, German Aerospace Center - DLR, Oberpfaffenhofen, Germany

ABSTRACT

A geostatistical analysis of the atmospheric phase screen (APS) affecting Ku-Band terrestrial radar interferometric (TRI) observations of a fast-flowing alpine glacier is made assuming a separable spatio-temporal covariance structure. Such a structure facilitates the mitigation of APS: the atmospheric phase affecting individual interferograms can be extrapolated form a set of persistent scatterers (PS) using regression-Kriging. After removing this estimate the residual APS is only correlated in time; its effect on surface displacement estimation is mitigated with a generalized least squares (GLS) inversion employing an estimate of the temporal covariance of the APS. The applicability of a separable covariance structure and the performance of the APS correction method are assessed on a TRI timeseries of Bisgletscher, a glacier in the southwestern Swiss Alps.

1. INTRODUCTION

Terrestrial Radar Interferometry (TRI) can be used to monitor displacements in natural terrain[1], [2] at day and night, regardless of weather. Typical applications are the observation of instable slopes[3], rock glaciers and glaciers[4]–[6]. Terrestrial radar interferometers are very suitable for those applications requiring zero-baseline differential interferometry as they provide great flexibility in the acquisition geometry and timing.

Differential interferometry is a coherent method: the phase of a target in a radar acquisition is proportional to its distance to the radar; when acquisitions at different times are combined in an interferogram, the phase difference is is proportional to the displacement of the target. However, the phase is also affected by changes in the refraction index of the propagation medium, which are usually due to variations in the spatial distribution of atmospheric water vapor content. This signal is superimposed to the displacement phase and is of comparable magnitude, reducing the accuracy of estimated displacements. However APS and displacement have different spatio-temporal behaviors, permitting statistical inferences regarding their relative contributions, particularly if multiple interferograms are used for the estimation[7].

2. METHODS

2.1. Signal Model

The problem of estimating terrain displacements given a set of M interferograms each consisting of P pixels can be written as[8]:

$$\mathbf{z} = \frac{4\pi}{\lambda}\mathbf{T}\mathbf{v} + \epsilon_{atm} + \epsilon_{decorr} \tag{1}$$

where $\mathbf{z}$ is a $P\ M$ vector of unwrapped, referenced interferometric phases obtained from a vector $\mathbf{y}$ of $P\ N$ SLC phases ordered by time of acquisition. The two vectors are related through the incidence matrix $\bar{\mathbf{A}}$[8]:

$$\mathbf{z} = \bar{\mathbf{A}}\mathbf{y}. \tag{2}$$

where $\bar{\mathbf{A}}$ indicates that the incidence matrix is a block diagonal matrix built of P identical $M \times N$ blocks. $\mathbf{v}$ is a vector of $P\ S, S \leq M$ velocities at S times and $\mathbf{T}$ is a block-diagonal matrix with blocks of size $M \times S$. Each block in $\mathbf{T}$, corresponding to a pixel in the interferogram stack consists of the same matrix: its i-th column is the vector of temporal baselines for the M/S interferograms in $\mathbf{z}$ for which a constant displacement velocity v_i is assumed for that pixel. As an example, assuming a single velocity v for each pixel for the entire stack duration ($S = M$) corresponds to interferogram stacking[9].

Finally, ϵ_{atm} is the atmospheric phase (APS) and ϵ_{decorr} represents other sources of noise such as thermal noise and temporal decorrelation. Both these contributions are assumed to be zero-mean Gaussian random vectors with covariance matrix $\mathbf{\Sigma} = \mathbf{\Sigma}_{atm} + \mathbf{\Sigma}_{decorr}$.

The best linear unbiased (BLUE) estimate of the velocity vector $\mathbf{v}$ from the interferogram stack $\mathbf{z}$ is the generalized least squares solution:

$$\hat{\mathbf{v}} = \left(\mathbf{T}^T\mathbf{\Sigma}^{-1}\mathbf{T}\right)^{-1}\mathbf{T}^T\mathbf{\Sigma}^{-1}\mathbf{z}. \tag{3}$$

However the covariance matrix $\mathbf{\Sigma}$ is usually not known; even if it were its large size would make the solution of (3) impractical.

2.2. Covariance Model and Inversion Strategy

Instead of directly computing (1), a two-step inversion scheme can be employed.
To do so, ϵ_{atm} the APS affecting each SLC acquisition in $\mathbf{y}$ is decomposed in two terms: a stratified APS contribution $\epsilon_{y,atm,strat}$ and a turbulent APS $\epsilon_{y,atm,turb}$. The former is used to describe atmospheric layering[4], [10]; it is described with a multiple regression model using functions of the pixel's locations. The turbulent APS is assumed to be a zero mean, second order spatially and temporally stationary Gaussian random process with separable spatio-temporal covariance structure[11]: its covariance can be written as the Kronecker product of spatial $\mathbf{\Sigma}_{atm,s}$ and temporal covariance matrices $\mathbf{\Sigma}_{atm,t}$. The covariance of the *differential* APS observed in the interferogram vector is then [7]:

$$\begin{aligned}\mathbf{\Sigma}_{atm} &= \bar{\mathbf{A}}\left(\mathbf{\Sigma}_{atm,s} \otimes \mathbf{\Sigma}_{atm,t}\right)\bar{\mathbf{A}}^T \\ &= \mathbf{\Sigma}_{atm,s} \otimes \left(\mathbf{A}\mathbf{\Sigma}_{atm,t}\mathbf{A}^T\right)\end{aligned} \tag{4}$$

In spaceborne InSAR $\mathbf{\Sigma}_{atm,t} = \mathbf{I}$ is usually assume: successive passes are separated by several days or longer, which ensures uncorrelated atmospheric turbulence. This assumption does not necessarily apply to TRI observations, where the repeat time is much shorter. Possible correlations in time are allowed through a non-diagonal $\mathbf{\Sigma}_{atm,t}$.
Spatio-temporal separability implies that spatial and temporal covariance structures are independent of each other and are respectively functions of spatial and temporal separations: the spatial covariance structure cannot change as a function of time[7]. The only way time can affect the spatial covariance is by changing its overall magnitude as a function of the temporal baseline. Thus the APS in two interferograms with different spatial baselines will have the same spatial correlation structure; only their phase variance can differ.
The decorrelation process $\mathbf{\Sigma}_{decorr}$ is assumed to be spatially uncorrelated and can estimated using the procedure described in [7].
The above model is used to estimate the solution of equation (1) in the following manner:

- Identify a set of persistent scatterers (PS) where $\mathbf{v} = 0$. The selection of the PS usually proves to be unproblematic in the case of alpine glaciers: The locations affected by displacement are normally known a priori and can be easily masked out; other deformation processes outside of that region happen at widely different timescales. With these PS a second interferogram stack is computed which is virtually free of deformation and decorrelation contributions.

- Estimate $\mathbf{\Sigma}_{atm,s}$ and $\mathbf{\Sigma}_{atm,t}$ using variogram analysis on the PS stack. $\mathbf{\Sigma}_{atm,s}$ is obtained by averaging spatial variograms computed on individual interferograms, assuming spatio-temporal separability. Similarly, $\mathbf{\Sigma}_{atm,t}$ is computed as the square average of unwrapped interferometric phase differences binned by temporal baseline.

- Extrapolate the phases at the PS to the locations of the interferogram $\mathbf{z}$ using regression-Kriging (RK)[12] with a model of APS stratification and the estimated spatial variogram. This gives a 2D prediction of the spatially correlated APS which can be removed from the interferogram. The residual interferogram vector $\mathbf{z}_{res}$ is then approximatively spatially uncorrelated.

- Compute the Generalized Least Squares (GLS) estimate (3) of $\mathbf{v}$ using $\mathbf{z}_{res}$ instead of $\mathbf{z}$. The GLS inverse can be computed pixel by pixel: the APS correction using RK makes $\mathbf{z}_{res}$ approximately uncorrelated in space.

3. DATA

The methods described above are tested with a dataset acquired using KAPRI (Ku-Band Advanced Polarimetric Radar Interferometer)[13], a polarimetric extension of the GPRI[14] real aperture TRI operating at 17.2 GHz.
The data was acquired during the summer months of 2015 in the Mattertal, Southwestern Swiss Alps, canton of Valais during a campaign to monitor Bisgletscher, a steep, fast flowing –up to 2 meters/day in its fastest parts– glacier near the village of Randa.
In the course of the campaign a timeseries of SLC images spaced 2:30 minutes apart was acquired; from which 10 dates are chosen randomly as reference dates. The random sampling ensures that SLCs representing different atmospheric conditions are analyzed.
Variogram analysis is performed on the set of all interferograms with a temporal baseline less than one hour from the references; while GLS inversion to derive velocity maps is applied on all the interferometric pairs with a maximum temporal baseline of 5 minutes. The threshold is chosen to minimize phase wraps and temporal decorrelationn. A model assuming a constant velocity over the course of 30 minutes ($S = 15$) was chosen for the GLS inversion.

4. RESULTS

Figure 1 is used to test the separability of the APS covariance by computing experimental variograms using interferograms from different dates and increasing temporal baselines; these are encoded in the point's color in the plot; the mean variogram is shown as a dashed line while the variance in the spatial semivariance across all interferograms is displayed as a gray ribbon. The blue line indicates a fitted exponential variogram model that is employed to extrapolate the APS observed at the PS using regression-Kriging (RK), which predicts the APS considering the spatial statistics and the APS

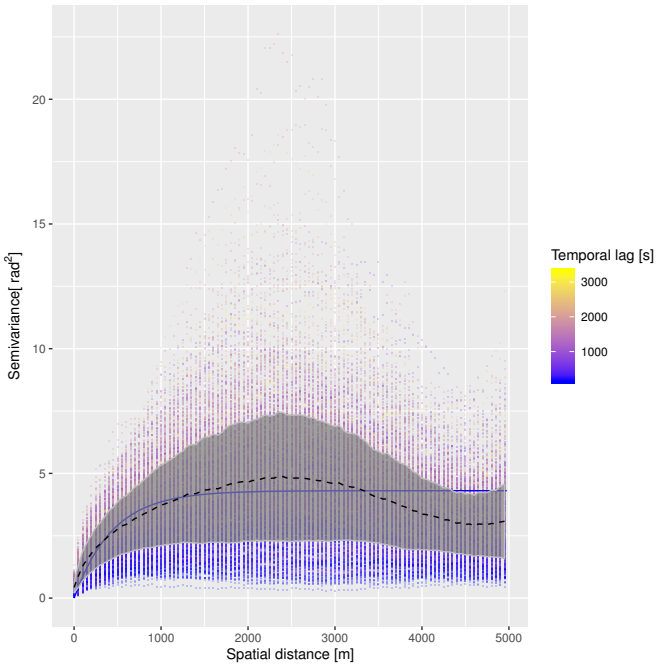

Fig. 1. Experimental spatial variogram; each dot shows the semivariance for an interferogram at a given spatial separation; the temporal lag is given by the dot's color; the dashed black line shows the variogram obtained by averaging the semivariance over all interferograms while the gray surface displays the standard deviation. The blue line is a fitted exponential variogram model.

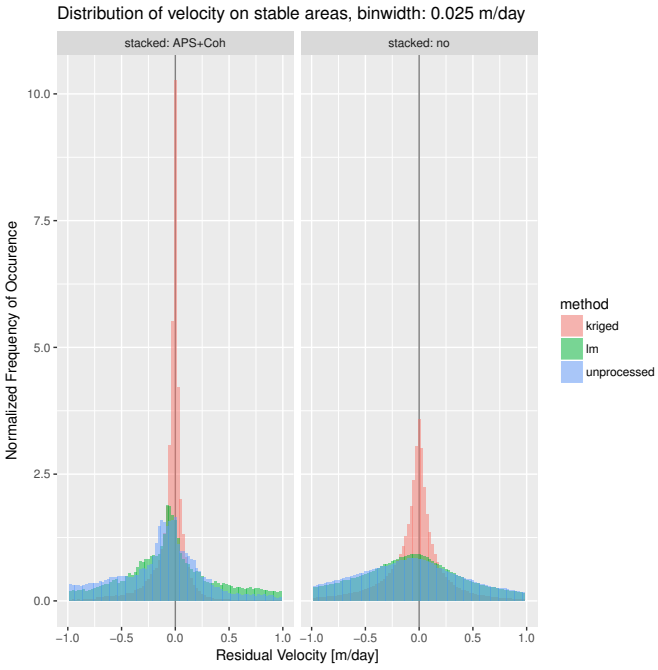

Fig. 2. Cross-validation of APS correction and inversion performance: the estimated velocities on a set of stable locations, where no displacements are expected ($\mathbf{v} = 0$) are extracted and their distribution plotted as an histogram. The column named *stacked: no* on the right shows the solutions obtained by applying APS correction methods (*kriged*: RK, *lm*: Stratified model only, *unprocessed*: no correction) to the interferograms and converting their phases into velocities; the column *APS+Coh* on the left display the distribution of estimates obtained with the same APS correction methods followed by GLS inversion.

stratification model simultaneously. The performance of RK is evaluated by cross-validation: the RK prediction of the APS is computed for each interferogram to derive the residual interferogram $\mathbf{z}_{res}$. A second set of PS located on stable areas in proximity of the glacier, where $\mathbf{v} = 0$ is expected, is used to extract the residual phases after RK, which are converted into line of sight velocities; they are shown in the form of residual velocity histograms in Figure 2.

Finally, an example displacement map obtained using RK correction and GLS inversion is displayed in Figure 2, overlaid to a topographic map.

5. DISCUSSION

Separability seems a reasonable assumption considering the moderate difference between variograms computed from individual interferograms, as shown by the gray ribbon of Figure 1. Assuming the covariance to be separable, the spatial variograms must be the same up to a scaling factor and offset for all temporal baselines.

However, variations in variogram's shape are still observed in the plot; they may relate to non-stationarity in the atmospheric turbulence caused by varying weather conditions and amount of solar radiation at different dates and times of the day.

A significant reduction in phase variance compared to the unprocessed interferograms (label *method: unprocessed*) is observed when the RK APS predictions are subtracted (label *method: kriged*). Removing only the stratified APS predicted by the multiple regression model (label *method: lm*) does not substantially reduce phase variance. This observation was tested quantitatively by computing the statistics of R^2 over all runs of the multiple regression APS model, giving an average R^2 of 0.2, suggesting that most of the phase variance is to be attributed to turbulence of the APS and not to atmospheric stratification.

When regression-Kriging is combined with GLS estimation of the velocities an additional decrease in variance is achieved, as shown in the left column named *stacked: APS+Coh* of Figure 2.

The estimated velocities are in agreement with the current knowledge on the Bisgletscher, where time-lapse camera ob-

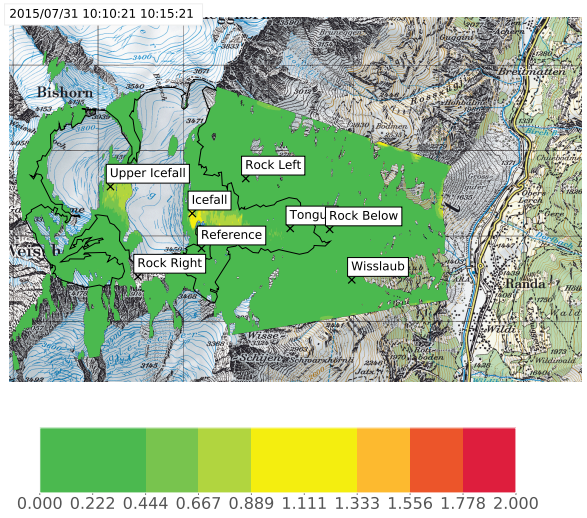

Fig. 3. Example displacement map obtained using spatial APS correction with RK plus GLS inversion weighted by the temporal covariance of the APS. The outline of the Bisgletscher is shown in black. Areas of low coherence or located in radar shadows are masked. The times correspond to the first and last acquisition used in the stack.

servations gave estimated flow velocities of up to 2 m/day in the fastest parts.

References

[1] R. Caduff, F. Schlunegger, A. Kos, and A. Wiesmann, "A review of terrestrial radar interferometry for measuring surface change in the geosciences," *Earth Surface Processes and Landforms*, vol. 40, no. 2, pp. 208–228, 2015.

[2] R. Iglesias, A. Aguasca, X. Fabregas, J. J. Mallorqui, D. Monells, C. Lopez-Martinez, and L. Pipia, "Ground-based polarimetric SAR interferometry for the monitoring of terrain displacement phenomena-part I: theoretical description," *IEEE Journal of Selected Topics in Applied Earth Observations and Remote Sensing*, vol. 8, no. 3, pp. 1–1, 2014.

[3] R. Caduff and T. Strozzi, "Terrestrial Radar Interferometry Monitoring During a Landslide Emergency 2016, Ghirone, Switzerland," in *Advancing Culture of Living with Landslides: Volume 3 Advances in Landslide Technology*, M. Mikoš, Ž. Arbanas, Y. Yin, and K. Sassa, Eds. Cham: Springer International Publishing, 2017, pp. 301–309.

[4] D. Mecatti, L. Noferini, G. Macaluso, M. Pieraccini, G. Luzi, C. Atzeni, and A. Tamburini, "Remote sensing of glacier by ground-based radar interferometry," *International Geoscience and Remote Sensing Symposium (IGARSS)*, pp. 4501–4504, 2007.

[5] N. Dematteis, G. Luzi, D. Giordan, F. Zucca, and P. Allasia, "Monitoring Alpine glacier surface deformations with GB-SAR," *Remote Sensing Letters*, vol. 8, no. 10, pp. 947–956, 2017.

[6] L. Noferini, D. Mecatti, G. Macaluso, M. Pieraccini, and C. Atzeni, "Monitoring of Belvedere Glacier using a wide angle GB-SAR interferometer," *Journal of Applied Geophysics*, vol. 68, no. 2, pp. 289–293, 2009.

[7] P. S. Agram and M Simons, "A noise model for InSAR time series," *Journal of Geophysical Research : Solid Earth*, no. May 2014, pp. 1–20, 2015.

[8] R. Lanari, F. Casu, M. Manzo, G. Zeni, P. Berardino, M. Manunta, and A. Pepe, "An overview of the Small BAseline Subset algorithm: A DInSAR technique for surface deformation analysis," in *Pure and Applied Geophysics*, 4, vol. 164, Basel: Birkhäuser Basel, 2007, pp. 637–661.

[9] T. R. Emardson, M Simons, and F. H. Webb, "Neutral atmospheric delay in interferometric synthetic aperture radar applications: Statistical description and mitigation," *Journal of Geophysical Research: Solid Earth*, vol. 108, no. B5, p. 2231, 2003.

[10] R. Iglesias, X. Fabregas, A. Aguasca, J. J. Mallorqui, C. Lopez-Martinez, J. A. Gili, and J. Corominas, "Atmospheric phase screen compensation in ground-based sar with a multiple-regression model over mountainous regions," *IEEE Transactions on Geoscience and Remote Sensing*, vol. 52, no. 5, pp. 2436–2449, 2014.

[11] T. Gneiting, M. Genton, and P. Guttorp, "Geostatistical Space-Time Models, Stationarity, Separability, and Full Symmetry," in *Statistical Methods for Spatio-Temporal Systems*, 2006, pp. 151–175.

[12] R. S. Bivand, E. J. Pebesma, and V. Gómez-Rubio, "Applied Spatial Data Analysis with R," in *Use R*, vol. 1, 2013, p. 378.

[13] S. Baffelli, O. Frey, C. Werner, and I. Hajnsek, "Polarimetric Calibration of the Ku-Band Advanced Polarimetric Radar Interferometer," *IEEE Transactions on Geoscience and Remote Sensing*, vol. 56, no. 4, pp. 2295–2311, 2018.

[14] C. Werner, A. Wiesmann, T. Strozzi, A. Kos, R. Caduff, and U. Wegmüller, "The GPRI multi-mode differential interferometric radar for ground-based observations," in *Proceedings of the European Conference on Synthetic Aperture Radar*, VDE, 2012, pp. 304–307.